Optical Imaginary Directional Couplers

Shaolin Ke, Dong Zhao, Qingjie Liu, Shun Wu, Bing Wang ⓘ, and Peixiang Lu, *Fellow, OSA*

Abstract—We investigate the light propagation in a double-waveguide coupler with imaginary-valued coupling coefficient. The imaginary coupling is realized by incorporating an additional waveguide between the coupled waveguides and considering both gain and loss. Both symmetric and asymmetric couplers with imaginary coupling are analyzed. The coupling strength can be controlled by varying the dielectric gain and loss. As the coupling is imaginary, the energy of the system is no longer conserved and the light intensities in individual waveguides should oscillate in phase. It is also found that the exceptional points can emerge in the asymmetric couplers, which are reflected from the beat length of the intensity oscillation. The study may find great applications in optical switches and splitters.

Index Terms—Exceptional point, imaginary coupling, optical waveguides.

I. INTRODUCTION

OPTICAL coupled waveguides have attracted considerable attention as they may find application in optical switches, routing, and power dividers [1]–[7]. They can be also utilized to demonstrate optical analogues of semiclassical electron dynamics [8], [9], such as Bloch oscillations [10]–[12] and topological edge states [13]–[19]. Recent interest has focused on non-Hermitian systems with gain and loss [19]–[21], which may yield complex propagation constants. So far, many fascinating phenomena have been observed in coupled waveguides by alternating the imaginary parts of propagation constants [22]–[24]. For example, double refraction is found in parity-time (PT)
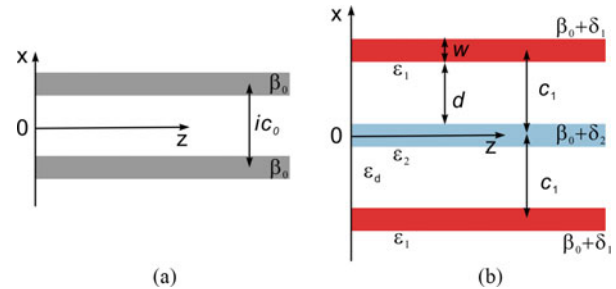
Fig. 1. Schematic of imaginary couplers. (a) The supposed coupler with imaginary coupling. (b) The proposed structures to realize effective imaginary coupling for outer two waveguides. Light propagates along the z axis.

symmetric waveguide arrays due to the non-orthogonal eigenmodes [25]. Loss induced transparency is observed in the vicinity of exceptional points (EPs) [23], which are the degeneracies of non-Hermitian system with two eigenvalues and eigenstates coalescing. In a PT-symmetric coupler, light propagates in a non-reciprocal manner both below and above the PT-symmetric threshold [26]. The loss induced amplification and localization are proposed in the realm of graphene plasmonic waveguides [27]–[30].

In spite of the complex propagation constants, the coupling coefficient between adjacent waveguides might be real in non-Hermitian waveguides. Many efforts have been paid to change the sign of coupling in order to modulate the flow of light [31]–[33]. The negative coupling is realized by inserting an ancillary waveguide [31] or utilizing sinusoidal curved waveguides [32]. The complex couplings can be achieved by embedding amplifying or lossy media between adjacent waveguides [34] or periodically modulating the gain and loss [35], which may slow down the light diffraction [36] and allow bound states [37] and flat bands [38] exist in photonic lattices. It remains an interesting issue to explore the light propagation in directional couplers governed by complex couplings.

In this work, we propose a method to realize imaginary coupling in a double-waveguide coupler, by inserting an ancillary waveguide and carefully setting the dielectric gain and loss. Both symmetric and asymmetric imaginary couplers are discussed. The coupled-mode theory and the numerical simulation are performed to reveal the optical features of the couplers with imaginary coupling.

II. SYMMETRIC DIRECTIONAL COUPLERS

Fig. 1(a) shows the schematic diagram of the two evanescently coupled waveguides with imaginary coupling. The two waveguides are identical with both propagation constants

denoted by β_0. The coupling coefficient is imaginary and labeled as ic_0. The light propagates along the z axis with the amplitude $\mathbf{A}(z) = [A_1(z), A_2(z)]^T$, which is governed by coupled-mode theory. Throughout the study, the time dependence term is exp $(-i\omega t)$ with ω denoting frequency. Then, the coupled-mode equation is given by $-i\,d\mathbf{A}/\,dz = \mathbf{HA}$, where the system Hamiltonian reads as

$$\mathbf{H} = \begin{bmatrix} \beta_0 & ic_0 \\ ic_0 & \beta_0 \end{bmatrix} \tag{1}$$

The system is non-Hermitian as the off diagonal elements are not conjugate. The eigenvalues of (1) stands for the propagation constants of the supermodes, which read

$$\beta_\pm = \beta_0 \pm ic_0 \tag{2}$$

The corresponding eigenvectors are $\mathbf{A}_+ = (1, 1)^T$ and $\mathbf{A}_- = [1, -1]^T$, which represent the symmetric and anti-symmetric modes, respectively. As the coupling strength is zero, that is, $c_0 = 0$, the system becomes Hermitian and the diabolic point emerges. The diabolic point is the singularity of spectrum as two eigenvalues coalesce but with different eigenvectors, which is also known as Dirac point in the momentum space [33].

In gainless and lossless waveguides, the coupling coefficients are real-valued as they are positive in dielectric waveguides and negative in metallic ones [33], [39]. The gain and loss in the waveguides will introduce nonzero imaginary parts to the coupling coefficient and the cross coupling coefficients turn to be asymmetric as they are conjugate to each other [23], [36], [40]. In the low-loss limit, the imaginary part of coupling coefficient is quite small when compared with the real part [40]. Therefore, these imaginary parts can be neglected and the coupling coefficients are approximately real and symmetric [19]. The imaginary-valued coupling coefficient can be realized by incorporating an additional waveguide into the coupler as shown in Fig. 1(b). The field amplitudes of the triplet are denoted by $\mathbf{B}(z) = [B_1(z), B_2(z), B_3(z)]^T$. The system Hamiltonian is written as

$$\mathbf{H} = \begin{bmatrix} \beta_0 + \delta_1 & c_1 & 0 \\ c_1 & \beta_0 + \delta_2 & c_1 \\ 0 & c_1 & \beta_0 + \delta_1 \end{bmatrix}. \tag{3}$$

where $\delta_{1,2}$ stand for the detuning of propagation constants, and c_1 is real and represents the coupling strength.

There are three supermodes in the triplet waveguides. The eigenvalues are given by

$$\begin{aligned} \beta_A &= \beta_0 + \delta_1, \\ \beta_B &= \beta_0 + \frac{\delta_1 + \delta_2}{2} - \sqrt{2c_1^2 + \left(\frac{\delta_1 - \delta_2}{2}\right)^2}, \\ \beta_c &= \beta_0 + \frac{\delta_1 + \delta_2}{2} + \sqrt{2c_1^2 + \left(\frac{\delta_1 - \delta_2}{2}\right)^2}, \end{aligned} \tag{4}$$

The corresponding eigenvectors can be taken as follows

$$\begin{aligned} \mathbf{B}_A &= \begin{pmatrix} -1 & 0 & 1 \end{pmatrix}^T, \\ \mathbf{B}_B &= \begin{pmatrix} 1 & -\frac{\delta_1 - \delta_2 + \sqrt{8c_1^2 + (\delta_1 - \delta_2)^2}}{2c_1} & 1 \end{pmatrix}^T, \\ \mathbf{B}_c &= \begin{pmatrix} 1 & -\frac{\delta_1 - \delta_2 - \sqrt{8c_1^2 + (\delta_1 - \delta_2)^2}}{2c_1} & 1 \end{pmatrix}^T. \end{aligned} \tag{5}$$

The ideal symmetric and anti-symmetric modes in ternary waveguide can be defined as $\mathbf{B}_+ = (1, 0, 1)^T$ and $\mathbf{B}_- = (-1, 0, 1)^T$, respectively. For the equivalence to achieve imaginary coupling, we have to ensure two of three eigenvalues and eigenvectors of triplet waveguide match that of the double-waveguide couplers, which can be realized according to the following steps. Firstly, we choose $\beta_A = \beta_0 - ic_0$ and $\beta_B = \beta_0 + ic_0$ to fulfill the matching of eigenvalues. Both condition are satisfied for

$$\delta_1 = -ic_1, \delta_2 = i(c_0^2 + c_1^2)/c_0 \tag{6}$$

We assume the imaginary coupling strength c_0 is positive. Then, (6) indicates the two side waveguides are with gain and the center waveguide is with loss. Secondly, we have to analysis the matching condition of eigenvectors to ensure $\mathbf{B}_A = \mathbf{B}_-$ and $\mathbf{B}_B = \mathbf{B}_+$. From (5), one can find the anti-symmetric mode $\mathbf{B}_A$ is perfect and remain unchanged as other parameters vary. Applying (6) into (5), one find $\mathbf{B}_B = [1, 2ic_0/c_1, 1]$, which is not expected as an imaginary component resides on the center waveguide. In order to quantify the similarity of symmetric mode, we can define the fidelity of field, which is given by

$$F = \left| \sum_j \mathbf{A}_j^+ \mathbf{B}_j^{+*} \right| \tag{7}$$

It is found that $F = [1 - 2(c_0/c_1)^2]^{-1/2}$ for the symmetric mode. The fidelity tends to be unity as the coupling satisfies the condition $|2c_0/c_1| \ll 1$. Finally, in this region, the eigenvalue and eigenvectors of third eigenmode are $\beta_c = \beta_0 + i(c_1^2 - c_0^2)/c_0$ and $\mathbf{B}_3 = [1, ic_1/c_0, 1]$, respectively. The mode is strongly decayed and the energy resides mostly on the center waveguide, which almost has no effect on the other side modes. Therefore, the imaginary coupler can be effectively realized for the two side waveguides.

Here we consider the InGaAsP waveguides to exam the features of complex coupling. The real part of permittivity of InGaAsP is $\varepsilon_0 = 12.25$. The optical gain can be generated by optical pumping, while the loss can be achieved by evaporating thin Cr layer on the waveguides. The waveguides are assumed to be suspended in air with $\varepsilon_d = 1$ for simplicity. The widths of waveguide and air are $w = 0.24\,\mu$m and $d = 0.5\,\mu$m, respectively. The incident wavelength is fixed at $\lambda = 1.55\,\mu$m. The parameters are chosen such that a waveguide only supports a single propagating mode of TM polarization. The propagation constants and field distributions can be calculated by utilizing transfer matrix method [41]. The propagation constant of single waveguide is figured out as $\beta_0 = 7.76\,\mu$m^{-1}. The simulation results show the complex propagation constants of single waveguide are $\beta \approx \beta_0 + 0.713i\,\Delta\varepsilon$ with $\Delta\varepsilon$ denoting the detuned imaginary part of permittivity of InGaAsP. The coupling between adjacent waveguides should exponential decrease with the increases of spacing and has the form $c_1 = a_0 \exp[-\kappa(d + w)]$ [35]. By fitting the propagation constants as a function of the distance, one can find that $a_0 = 2.65\,\mu$m^{-1} and $\kappa = 6.5\,\mu$m^{-1}. The interlayer space of the waveguides is chosen as $d = 0.5\,\mu$m and thus the coupling coefficient is $c_1 = 0.047\,\mu$m^{-1}. Then we can determine the detuned permittivity to construct the
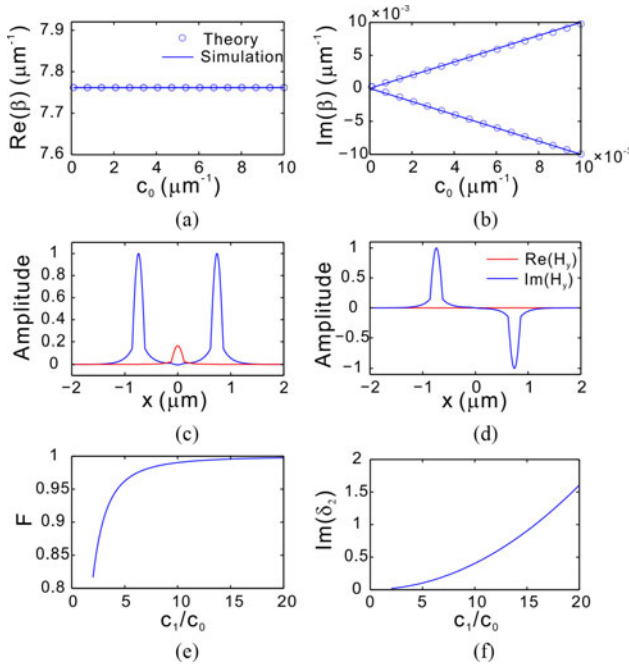
Fig. 2. The propagation constants and mode profiles of imaginary couplers. (a) and (b) Real and imaginary parts of propagation constants as coupling strength is varying. (c) and (d) Simulated mode profile for the symmetric and anti-symmetric modes, respectively. (e) Overlap of the symmetric matched eigenmodes of the triplet and the ideal imaginary coupler. (f) The required detuning of the central waveguide as a function of coupling c_1.
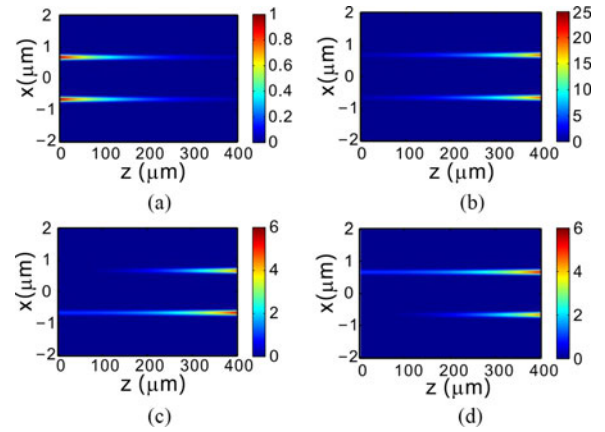

Fig. 3. Intensity distribution ($|\mathbf{H}|^2$) in the triplet for different excitation conditions: (a) symmetric mode, (b) anti-symmetric mode, (c) lower waveguide, and (d) upper waveguide. The field is normalized by the maximum of incident wave.

imaginary couplers. For example, as imaginary coupling strength is $c_0 = 4 \times 10^{-3}$ μm^{-1}, the additional propagation constants of outer waveguides should be $\delta_1 = -4i \times 10^{-3}$ μm^{-1}. Then the detuned propagation constants can be determined according to (6) as $\delta_2 = 0.56i$ μm^{-1}. Therefore, the additional imaginary permittivity of side and center waveguides should be $\Delta\varepsilon_1 = -5.6 \times 10^{-3}$ and $\Delta\varepsilon_2 = 0.79$. The different imaginary coupling strength can be acquired by tuning the detuned permittivity $\Delta\varepsilon_1$ and $\Delta\varepsilon_2$.

Fig. 2(a) and (b) illustrate the propagation constants as a function of the imaginary coupling strength. The line stands for the simulations for the triplet waveguides. The dots represent the indications for imaginary coupler according to (2). The real parts of propagation constants for symmetric and anti-symmetric modes remain unchanged as coupling c_0 increases. In contrast, the imaginary parts of symmetric and anti-symmetric modes show a linear increase and decrease, respectively. The simulation and theory agree well with each other. In Fig. 2(c) and (d), we plot the mode profiles for symmetric and anti-symmetric modes as $c_0 = 4 \times 10^{-3}$ μm^{-1}. For the anti-symmetrical mode, the fields are perfectly confined at outer two waveguides with gain and there is almost no energy on the middle lossy waveguide. Therefore, the anti-symmetric is amplified. However, for the symmetric mode, the energy is mostly confined at outer two waveguides with gain but also with field locating at the middle lossy waveguide. As the loss coefficient is about one hundred times larger than the gain coefficient of the outer waveguides, the little energy in middle waveguide could make the symmetric mode attenuated. On the other hand, the symmetric mode could

be amplified and the anti-symmetric mode decays by reversing the distributions of gain and loss.

The fidelity of symmetric mode is related to the coupling strength c_1 in triplet waveguide. Fig. 2(e) depicts the fidelity as a function of c_1 for $c_0 = 4 \times 10^{-3}$ μm^{-1}. The fidelity grows with the increases of ratio of coupling strength and tends to unity as $c_1/c_0 \to \infty$. However, the imaginary detuning of propagation constant is serious for larger ratio, as shown in Fig. 2(f). In this situation, it is hard to maintain the real part of propagation constants.

The mode propagation in the triplet waveguide system should be coincident with the imaginary coupler as the eigenvalues and eigenmodes of the two systems match well with each other. Fig. 3 shows the light propagation in the triplet waveguides for different excited conditions. The propagation is simulated using Rigorous coupled-wave analysis (RCWA) method [42]. In all cases, the effective imaginary coupling strength is fixed at $c_0 = 4 \times 10^{-3}$ μm^{-1}. Fig. 3(a) and (b) depict the propagation of symmetric and anti-symmetric modes, respectively. For symmetric mode, the energy decreases as propagation distance increase, while the energy increases for anti-symmetric mode. The energy is always dominated at outer waveguides for both cases, indicating that the wave propagation is coincident with that of the imaginary couplers. Here, we try to explain more about the propagation for symmetric injection. Mode B_c and B_b are simultaneously excited as a symmetrical mode is injected. For the parameter we choose, a symmetrical mode can be expanded as $0.9929 \times B_b + 0.119i \times B_c$ with B_b, and B_c being normalized eigenvectors. Obviously, the mode B_b dominates in both modes. Because mode B_c is attenuated faster than mode B_b, only mode B_b survives after propagating a certain distance.

The output amplitudes can be solved analytically according to the coupled mode theory [43], that is

$$\mathbf{A}(z) = \text{Exp}(i\beta_0 z) \begin{pmatrix} \cosh(c_0 z) & -\sinh(c_0 z) \\ -\sinh(c_0 z) & \cosh(c_0 z) \end{pmatrix} \mathbf{A}(0) \quad (8)$$
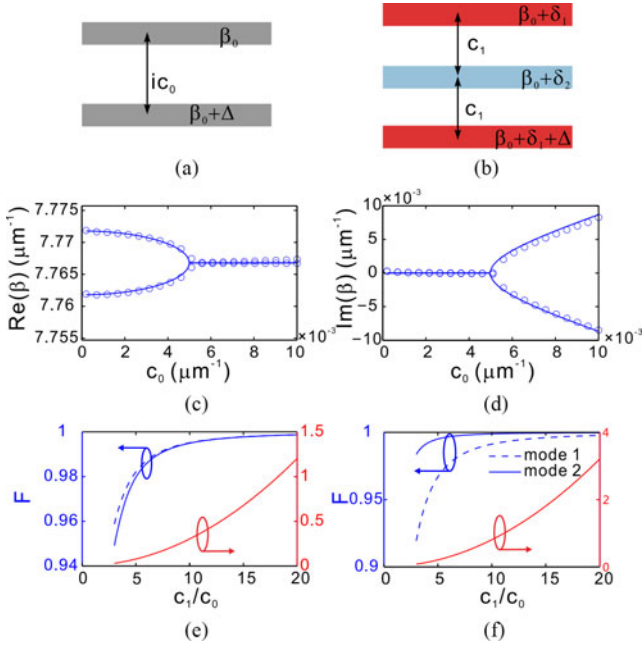
Fig. 4. (a) Schematic of supposed asymmetric directional couplers with imaginary coupling. (b) The proposed structures to realize effective imaginary coupling. (c) The real and (d) imaginary parts of propagation constants as a function of coupling strength. (e) and (f) Field fidelity and required detuning of the central waveguide versus coupling c_1, respectively.

where $\mathbf{A}(0) = [A_1(0), A_2(0)]^\mathrm{T}$ represents the initial excited conditions. The output intensities for the upper and lower waveguides are both $|A_{1,2}(z)|^2 = \exp(-2c_0 z)$ as the symmetric mode is injected. The output becomes $|A_{1,2}(z)|^2 = \exp(2c_0 z)$ as the initial condition changes to anti-symmetric mode. The analysis agrees well with the simulations shown in Fig. 3(a) and (b). It is well known that light intensity oscillates in conventional directional couplers with real coupling as a single waveguide is excited. In contrast, the intensities no longer oscillate but exponentially grow during propagation in the imaginary couplers. As the lower waveguide is excited with $\mathbf{A}(0) = [0, 1]$, the intensities in individual waveguides are $|A_1(z)|^2 = |\sinh(c_0 z)|^2$ and $|A_2(z)|^2 = |\cosh(c_0 z)|^2$, respectively. The output intensities tend to be equal as the ratio A_1/A_2 approaches unity for enough long propagation distance. The similar phenomenon is observed as the upper waveguide is excited. Fig. 3(c) and (d) show the wave propagation in the triplet waveguides as lower and upper waveguides are excited, respectively. The initial field can be regarded as the composition of symmetric and anti-symmetric modes, which amplitudes either exponentially decay or increase. Only the anti-symmetric mode effectively survives for long propagation distances. Therefore, the intensities in two waveguides tend to be equal at the output, which may be utilized to design stable optical dividers.

III. ASYMMETRIC DIRECTIONAL COUPLERS

The above method can be further used to develop the asymmetric directional couplers with imaginary coupling. Fig. 4(a) presents the schematic diagram of the asymmetric imaginary

coupler. The propagation constants of lower waveguide is larger than that of the upper with the detuning denoted by Δ, which is assumed to be real and positive. The system Hamiltonian is then written as

$$\mathbf{H} = \begin{bmatrix} \beta_0 & ic_0 \\ ic_0 & \beta_0 + \Delta \end{bmatrix} \qquad (9)$$

The eigenvalues of (9) are derived as

$$\beta_\pm = \beta_0 + \frac{\Delta}{2} \pm \sqrt{\frac{\Delta^2}{4} - c_0^2} \qquad (10)$$

The most prominent characteristic of the asymmetric couplers is that EPs can take place. An EP arises at the square-root branch point as two eigenvalues coalesce with $\beta_+ = \beta_-$. The condition is fulfilled as the detuning is twice as large as the coupling strength, that is, $\Delta = 2c_0$. The EPs are phase transition point as eigenmode show distinct behavior. Above the threshold $(2c_0 > \Delta)$, the eigenmodes are given by $[\pm \exp(i\theta), 1]^\mathrm{T}$ with $\sin(\theta) = \Delta/2c_0$. The absolute values of two elements are equal, indicating the energy is averagely distributed in two waveguides. At phase transition for $\Delta = 2c_0$, two modes coalesce to $[i, 1]^\mathrm{T}$, where the amplitudes in two waveguides have the same amplitude. Below the threshold $(2c_0 < \Delta)$, the eigenmodes becomes $[i\exp(\mp\theta), 1]$, where $\cosh(\theta) = \Delta/2c_0$. The energy tends to localize at a single waveguides. The asymmetric coupler with imaginary coupling can be also realized by placing an additional waveguide in the middle of the coupler, as shown in Fig. 4(b). The Hamiltonian of the triplet is given by

$$\mathbf{H} = \begin{bmatrix} \beta_0 + \delta_1 & c_1 & 0 \\ c_1 & \beta_0 + \delta_2 & c_1 \\ 0 & c_1 & \beta_0 + \delta_1 + \Delta \end{bmatrix}. \qquad (11)$$

The eigenvalues are $\beta_{1,2} \approx \beta_0 + \Delta/2 + (\Delta^2/4 + \delta_1^2)^{1/2}$ and $\beta_3 \approx c_1^2/\delta_1$ when $\delta_2 = c_1^2/\delta_1$ and $c_1 \gg \delta_2, \Delta$. The first two modes can be used to construct the asymmetric couplers with imaginary coupling by setting the detuning to be $\delta_1 = -ic_0$.

We now consider the InGaAsP waveguides to exam the features of asymmetric coupler with imaginary coupling. The additional permittivity of right waveguide is set to be $\Delta\varepsilon_3 = 0.014$ such that the detuning of the propagation constant is $\Delta = 0.01 \ \mu m^{-1}$. The other parameters keep unchanged. In Fig. 4(c) and (d), we plot the real and imaginary parts of the propagation constants as a function of imaginary coupling strength. The simulation and the theory agree well with each other. They share the characteristics of the square root. Increasing the coupling strength causes the propagation constants of the two modes to move towards each other to the critical point, that is, the branch point or called EP. Two propagation constants coalesce at $c_0 = \Delta/2$. The propagation constants become complex as $c_0 > \Delta/2$, and the systems support one gain- and one loss-guiding modes. In additional to the matching of the eigenvalues, the eigenmodes of triplet should also match that of the asymmetric coupler with imaginary coupling. Fig. 4(e) and (f) depict the field fidelity as a function of coupling strength c_1 as $c_0 = 2 \times 10^{-3} \ \mu m^{-1}$ and $6 \times 10^{-3} \ \mu m^{-1}$, which corresponds to the cases below and above EP, respectively. The fidelity grows
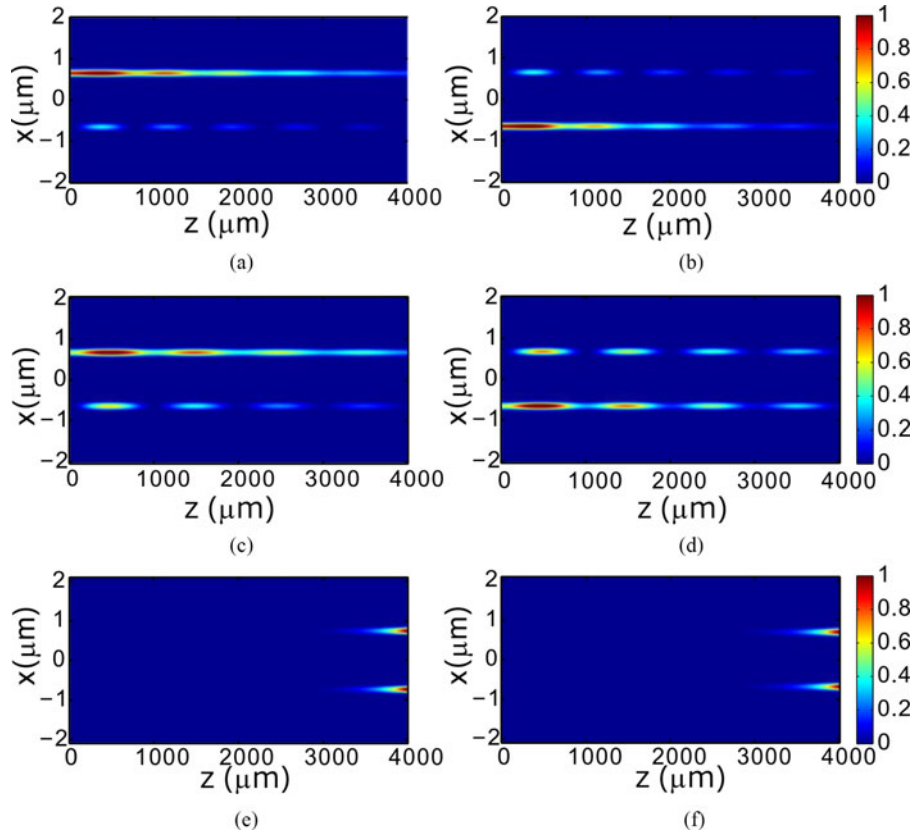
Fig. 5.   Intensity distribution ($|\mathbf{H}|^2$) for different coupling strength. (a) and (d) $c_0 = 3 \times 10^{-3}\,\mu m^{-1}$, (b) and (e) $c_0 = 4 \times 10^{-3}\,\mu m^{-1}$, and (c) and (f) $c_0 = 5.5 \times 10^{-3}\,\mu m^{-1}$. The light is injected from upper waveguide for (a)–(c) and lower waveguide for (d)–(f). The field is normalized by the maximum.

with the increases of ratio of coupling strength and tends to unity as $c_1/c_0 \to \infty$. Therefore, a larger ratio is desired to achieve better eigenmode matching. Similar to the case for a symmetric imaginary coupler, the imaginary detuning of propagation constants is large for a large ratio indicated by the red line shown in Fig. 4(e) and (f). As a result, it becomes challenging to keep the real part of propagation constants unchanged. Overall, the coupling strength should be properly designed.

We further investigate the light propagation in the asymmetric couplers with imaginary coupling. The light propagation shows distinct behavior below and above the threshold $2c_0 = \Delta$. Fig. 5 illustrates the simulated field intensity distributions in the triplet for three values of imaginary coupling strengths c_0. In Fig. 5(a)–(c), the light is launched from the upper waveguide. The center waveguide is always dark. Below the threshold, as shown in Fig. 5(a) and (b), the beat patterns are observed as light intensity oscillates during propagation. The intensities in the two waveguides always oscillate in phase as the wave intensities in individual waveguides always reach maximum or minimum at the same time. It is different from the conventional couplers with real coupling where the light intensity in one waveguide reaches maximum while approaches the minimum in the other one. The energy of upper waveguide is always larger than that of lower waveguide. The total energy slightly enlarges at first and then decreases with the increase of propagation distance. Moreover, the beat length increases as the coupling approaches the

critical value $2c_0 = \Delta$. When the EP is approached, the beat length goes to infinity. The field intensity no longer oscillates between the two side waveguides but rather travels in both waveguides simultaneously as shown in Fig. 5(c). Moreover, the total energy exponentially increases because the propagation constants are complex and only the amplifying mode survives. In this region, the intensities of two individual waveguides are identical. Therefore, the output energies in side waveguides tend to be of equal amplitude. Fig. 5(d)–(f) depict light propagation as lower waveguide is excited. Below the EP, one can also observe beating pattern. The fields at the output are mainly confined at lower waveguide. This is different from the case in Fig. 5(a) and (b) whereas the energy at upper waveguide is dominated. Above EP, the field intensity no longer oscillates and the output fields in upper and lower waveguides are almost of equal amplitudes, which is similar to the case for the excitation from upper waveguide.

IV. CONCLUSION

In conclusion, we have designed a double-waveguide coupler with imaginary coupling coefficient. The imaginary coupling is realized by incorporating an additional waveguide such that the wave vectors and eigenmodes of the triplet waveguide match well with that of the double-waveguide coupler with imaginary coupling. The method is valid to develop symmetric and

asymmetric couplers with imaginary coupling. We also show that the exceptional points (EPs) appear in the asymmetric couplers by varying the coupling strength. Below the EPs, the light intensities oscillate during propagation and the beat length increases when approaching EPs. Above the EPs, the light travels in both waveguides simultaneously and the output intensities in two waveguides tend to be identical. Our results provide a new way to design optical switches and splitters by taking advantage of the gain and loss present in the system.

REFERENCES

[1] W. P. Huang, "Coupled-mode theory for optical waveguides: An overview," *J. Opt. Soc. Amer. A, Opt., Image, Vis.*, vol. 11, no. 3, pp. 963–983, Aug. 1994.

[2] A. Locatelli, A. D. Capobianco, M. Midrio, S. Boscolo, and C. De Angelis, "Graphene-assisted control of coupling between optical waveguides," *Opt. Express*, vol. 20, no. 27, pp. 28479–28484, Dec. 2012.

[3] F. Gan, C. Sun, Y. Wang, H. Li, Q. Gong, and J. Chen, "Multimode metallic double-strip waveguides for polarization manipulation," *Adv. Mater. Technol.*, vol. 2, no. 4, Apr. 2017, Art. no. 1600248.

[4] Y. Xue, F. Ye, D. Mihalache, N. Panoiu, and X. Chen, "Plasmonic lattice solitons beyond the coupled-mode theory," *Laser Photon. Rev.*, vol. 8, no. 4, pp. 52–57, Jul. 2014

[5] Z. Wang, B. Wang, H. Long, K. Wang, and P. Lu, "Surface plasmonic lattice solitons in semi-infinite graphene sheet arrays," *J. Lightw. Technol.*, vol. 35, no. 14, pp. 2960–2965, May 2017.

[6] S. Wang, B. Wang, C. Qin, K. Wang, H. Long, and P. Lu, "Rabi oscillations of optical modes in a waveguide with dynamic modulation," *Opt. Quant. Electron.*, vol. 49, no. 389, pp. 1–8, Nov. 2017.

[7] C. Sun, K. Rong, Y. Wang, H. Li, Q. Gong, and J. Chen, "Plasmonic ridge waveguides with deep-subwavelength outside-field confinements," *Nanotechnology*, vol. 27, no. 6, Jan. 2016, Art. no. 065501.

[8] Y. N. Joglekar, C. Thompson, D. D. Scott, and G. Vemuri, "Optical waveguide arrays: Quantum effects and PT symmetry breaking," *Eur. Physical J. Appl. Phys.*, vol. 63, Jul. 2013, Art. no. 30001.

[9] F. Wang, C. Qin, B. Wang, H. Long, K. Wang, and P. Lu, "Rabi oscillations of plasmonic supermodes in graphene multilayer arrays," *IEEE J. Sel. Topics Quantum Electron.*, vol. 23, no. 1, Mar. 2017, Art. no. 4600105.

[10] U. Peschel, T. Pertsch, and F. Lederer, "Optical Bloch oscillations in waveguide arrays," *Opt. Lett.*, vol. 23, no. 21, pp. 1701–1703, 1998.

[11] A. Block *et al.*, "Bloch oscillations in plasmonic waveguide arrays," *Nature Commun.*, vol. 5, May 2014, Art. no. 3843.

[12] Y. Xu *et al.*, "Experimental realization of Bloch oscillations in a parity-time synthetic silicon photonic lattice," *Nature Commun.*, vol. 7, Apr. 2016, Art. no. 11319.

[13] F. Dreisow *et al.*, "Dirac dynamics in waveguide arrays: From Zitterbewegung to photonic topological insulators," in *Quantum Simulations With Photons and Polaritons*. New York, NY, USA: Springer, May 2017, pp. 181–214.

[14] Q. Cheng, Y. Pan, Q. Wang, T. Li, and S. Zhu, "Topologically protected interface mode in plasmonic waveguide arrays," *Laser Photon. Rev.*, vol. 9, no. 4, pp. 392–398, 2015.

[15] H. Deng, X. Chen, N. C. Panoiu, and F. Ye, "Topological surface plasmons in superlattices with changing sign of the average permittivity," *Opt. Lett.*, vol. 41, no. 18, pp. 4281–4284, Sep. 2016.

[16] F. Bleckmann, S. Linden, and A. Alberti, "Spectral imaging of topological edge states in plasmonic waveguide arrays," *Phys. Rev. B*, vol. 96, Jul. 2017, Art. no. 045417.

[17] L. Ge, L. Wang, M. Xiao, W. Wen, C. T. Chan, and D. Han, "Topological edge modes in multilayer graphene systems," *Opt. Express*, vol. 23, no. 17, pp. 21585–21595, Aug. 2015.

[18] F. Wang *et al.*, "Topological interface modes in graphene multilayer arrays," *Opt. Laser Technol.*, vol. 103, pp. 272–278, Jan. 2018.

[19] S. Weimann *et al.*, "Topologically protected bound states in photonic parity–time-symmetric crystals," *Nature Mater.*, vol. 16, no. 4, pp. 433–438, Apr. 2017.

[20] S. Klaiman, U. Gunther, and N. Moiseyev, "Visualization of branch points in PT-symmetric waveguides," *Phys. Rev. Lett.*, vol. 101, no. 8, Aug. 2008, Art. no. 080402.

[21] S. Ke, B. Wang, C. Qin, H. Long, K. Wang, and P. Lu, "Exceptional points and asymmetric mode switching in plasmonic waveguides," *J. Lightw. Technol.*, vol. 34, no. 22, pp. 5258–5262, Sep. 2016.

[22] B. Zhen *et al.*, "Spawning rings of exceptional points out of Dirac cones," *Nature*, vol. 525, no. 7569, pp. 354–358, Sep. 2015.

[23] A. Guo *et al.*, "Observation of PT-symmetry breaking in complex optical potentials," *Phys. Rev. Lett.*, vol. 103, no. 9, Aug. 2009, Art. no. 093902.

[24] S. Ke, B. Wang, H. Long, K. Wang, and P. Lu, "Topological mode switching in a graphene doublet with exceptional points," *Opt. Quant. Electron.*, vol. 49, no. 227, pp. 1–12, May 2017.

[25] K. G. Makris, R. El-Ganainy, and D. N. Christodoulides, "Beam dynamics in PT symmetric optical lattices," *Phys. Rev. Lett.*, vol. 100, Mar. 2008, Art. no. 103904.

[26] C. E. Rüter, K. G. Makris, R. El-Ganainy, D. N. Christodoulides, M. Segev, and D. Kip, "Observation of parity-time symmetry in optics," *Nature Phys.*, vol. 6, pp. 192–195, Mar. 2010.

[27] X. Lin *et al.*, "Loss induced amplification of graphene plasmons," *Opt. Lett.*, vol. 41, no. 4, pp. 681–684, 2016.

[28] X. Lin, N. Rivera, J. J. López, I. Kaminer, H. Chen, and M. Soljačić, "Tailoring the energy distribution and loss of 2D plasmons," *New J. Phys.*, vol. 18, no.10, Oct. 2016, Art. no. 105007.

[29] H. Huang, S. Ke, B. Wang, H. Long, K. Wang, and P. Lu, "Numerical study on plasmonic absorption enhancement by a rippled graphene sheet," *J. Lightw. Technol.*, vol. 35, no. 2, pp. 320–324, Dec. 2017.

[30] D. Zhao, Z. Wang, H. Long, K. Wang, B. Wang, and P. Lu, "Optical bistability in defective photonic multilayers doped by graphene," *Opt. Quant. Electron.*, vol. 49, no. 163, pp. 1–9, Mar. 2017.

[31] R. Keil *et al.*, "Universal sign control of coupling in tight-binding lattices," *Phys. Rev. Lett.*, vol. 116, May 2016, Art. no. 213901.

[32] J. M. Zeuner *et al.*, "Optical analogues for massless Dirac particles and conical diffraction in one dimension," *Phys. Rev. Lett.*, vol. 109, Jul. 2012, Art. no. 023602.

[33] S. Hyun Nam, A. J. Taylor, and A. Efimov, "Diabolical point and conical-like diffraction in periodic plasmonic nanostructures," *Opt. Express*, vol. 18, no. 10, pp. 10120–10126, 2010.

[34] N. V. Alexeeva, I. V. Barashenkov, K. Rayanov, and S. Flach, "Actively coupled optical waveguides," *Phys. Rev. A*, vol. 89, Jan. 2014, Art. no. 013848.

[35] S. Longhi, "Exceptional points and Bloch oscillations in non-Hermitian lattices with unidirectional hopping," *Europhys. Lett.*, vol. 106, no. 3, Feb. 2016, Art. no. 022102.

[36] M. Golshani *et al.*, "Impact of loss on the wave dynamics in photonic waveguide lattices," *Phys. Rev. Lett.*, vol. 113, Sep. 2014, Art. no. 123903.

[37] S. Longhi, "Non-Hermitian tight-binding network engineering," *Phys. Rev. A*, vol. 93, Feb. 2016, Art. no. 022102.

[38] D. Leykam, S. Flach, and Y. D. Chong, "Flat bands in lattices with non-Hermitian coupling," *Phys. Rev. B*, vol. 96, Aug. 2017, Art. no. 064305.

[39] A. Yariv and P. Yeh, *Optical Waves in Crystals*. Hoboken, NJ, USA: Wiley, 1984.

[40] Y. Li, X. Guo, C. Xu, J. Yang, X. Jiang, and M. Wang, "Coupled mode theory under the parity-time symmetry frame," *J. Lightw. Technol.*, vol. 31, no. 15, pp. 2477–2481, Aug. 2013.

[41] P. Yeh, *Optical Waves in Layered Media*. New York, NY, USA: Wiley, 1988.

[42] M. G. Moharam and T. K. Gaylord, "Rigorous coupled-wave analysis of planar-grating diffraction," *J. Opt. Soc. Amer.*, vol. 71, no. 7, pp. 811–818, Feb. 1981.

[43] C. Qin, B. Wang, H. Long, K. Wang, and P. Lu, "Nonreciprocal phase shift and mode modulation in dynamic graphene waveguides," *J. Lightw. Technol.*, vol. 34, no. 16, pp. 3877–3883, Aug. 2016.

Shaolin Ke received the B.S. degree and the Ph.D. degree in physics from the Huazhong University of Science and Technology, Wuhan, China, in 2013 and 2017, respectively. He is currently a Lecturer with the Wuhan Institute of Technology, Wuhan, China. His research interests include graphene plasmonics, dynamical modulation, and non-Hermitian waveguides.

Dong Zhao received the B.C. degree in applied physics from Chongqing University, Chongqing, China, in 2004, and the M.S. degree in theoretical physics from the Huazhong University of Science and Technology, Wuhan, China, in 2007. He is currently working toward the Ph.D. degree in optical engineering at the Huazhong University of Science and Technology. He is also a Lecturer with the School of Electronics Information and Engineering, Hubei University of Science and Technology. His research interests include nonlinear optics and photonic crystal.

Qingjie Liu received the B.S. degree in physics from Shandong University, Weihai, China, in 2015. She is currently working toward the Ph.D. degree in Physics, Huazhong University of Science and Technology. Her research interests include graphene plasmonics, non-Hermitian waveguides, and dynamic photonic devices.

Shun Wu received the B.S. degree in physics from Beijing Normal University, Beijing, China, in 2005, and the Ph.D. degree in physics from Kansas State University, Manhattan, KS, USA, in 2014. She is currently a Lecturer with the Wuhan Institute of Technology, Wuhan, China. Her current research interests include fiber lasers, frequency comb, fiber sensors, and ultrafast optics.

Bing Wang received the B.S. degree and the Ph.D. degree in physics from Wuhan University, Wuhan, China, in 2002 and 2007, respectively. He is currently a Professor with the School of Physics and the Wuhan National Laboratory for Optoelectronics, Huazhong University of Science and Technology, Wuhan, China. His current research interests include metal/graphene plasmonics, nanophotonics, and nonlinear and ultrafast optics.

Peixiang Lu received the B.S. degree in physics from Peking University, Beijing, China, in 1987, and the Ph.D. degree from the Shanghai Institute of Optics and Fine Mechanics, Chinese Academy of Sciences, Shanghai, China, in 1992. He is currently a Professor with the School of Physics and the Wuhan National Laboratory for Optoelectronics, Huazhong University of Science and Technology, Wuhan, China. His current research interests include ultrafast optics, laser physics and nanophotonics. He is a Fellow of the Optical Society of America.